Photochemistry and Photobiology, 2006, 82: 887–897

Symposium-in-Print: UV Effects on Aquatic and Coastal Ecosytems

Ultraviolet-B Radiation Effects on the Structure and Function of Lower Trophic Levels of the Marine Planktonic Food Web

Gustavo A. Ferreyra*[1,3], Behzad Mostajir[2], Irene R. Schloss[3,4], Khaled Chatila[1], Martha E. Ferrario[5], Peggy Sargian[1], Suzanne Roy[1], Johann Prod'homme[1] and Serge Demers[1]

[1]Institut des sciences de la mer de Rimouski, Université du Québec à Rimouski, 310 Allée des Ursulines, Rimouski (Québec) Canada G5L 3A1
[2]Réseaux Trophiques Pélagiques (CNRS-GDR 2476), UMR 5119 "Ecosystèmes lagunaires," CNRS-Université Montpellier II. Place E. Bataillon, 34095 Montpellier, France
[3]Instituto Antártico Argentino, Cerrito 1248 (1010), Buenos Aires, Argentina
[4]CONICET, Argentina
[5]Facultad de Ciencias Naturales y Museo de La Plata, Paseo del Bosque S/N 1900 La Plata, Argentina

Received 22 February 2006; accepted 24 May 2006; published online 26 May 2006 DOI: 10.1562/2006-02-23-RA-810

ABSTRACT

The impact of UV-B radiation (UVBR; 280–320 nm) on lower levels of a natural plankton assemblage (bacteria, phytoplankton and microzooplankton) from the St. Lawrence Estuary was studied during 9 days using several immersed outdoor mesocosms. Two exposure treatments were used in triplicate mesocosms: natural UVBR (N treatment, considered as the control treatment) and lamp-enhanced UVBR (H treatment, simulating 60% depletion of the ozone layer). A phytoplankton bloom developed after day 3, but no significant differences were found between treatments during the entire experiment for phytoplankton biomass (chlorophyll *a* and cell carbon) nor for phytoplankton cell abundances from flow cytometry and optical microscopy of three phytoplankton size classes (picoplankton, nanoplankton and microplankton). In contrast, bacterial abundances showed significantly higher values in the H treatment, attributed to a decrease in predation pressure due to a dramatic reduction in ciliate biomass (~70–80%) in the H treatment relative to the N treatment. The most abundant ciliate species were *Strombidinium* sp., *Prorodon ovum* and *Tintinnopsis* sp.; all showed significantly lower abundances under the H treatment. *P. ovum* was the less-affected species (50% reduction in the H treatment compared with that of the N control), contrasting with ~90% for the other ones. Total specific phytoplanktonic and bacterial production were not affected by enhanced UVBR. However, both the ratio of primary to bacterial biomass and production decreased markedly under the H treatment. In contrast, the ratio of phytoplankton to bacterial plus ciliate carbon biomass showed an opposite trend than the previous results, with higher values in the H treatment at the end of the experiment. These results are explained by the changes in the ciliate biomass and suggest that UVBR can alter the structure of the lower levels of the planktonic community by selectively affecting key species. On the other hand, linearity between particulate organic carbon (POC) and estimated planktonic carbon was lost during the postbloom period in both treatments. On the basis of previous studies, our results can be attributed to the aggregation of carbon released by cells to the water column in the form of transparent exopolymer particles (TEPs) under nutrient limiting conditions. Unexpectedly, POC during such a period was higher in the H treatment than in controls. We hypothesize a decrease in the ingestion of TEPs by ciliates, in coincidence with increased DOC release by phytoplankton cells under enhanced UVBR. The consequences of such results for the carbon cycle in the ocean are discussed.

INTRODUCTION

UV-B radiation (UVBR, 280–320 nm) is strongly absorbed by the stratospheric ozone layer, contrasting with most UV-A radiation (UVAR, 320–400 nm) and photosynthetically active radiation (PAR, 400–700 nm). The biological effects of enhanced UVBR, resulting from the breakdown of stratospheric ozone by chlorofluorocarbons (CFCs) and halons, has been a main scientific concern since the late 1970s (1). A significant quantity of information has accumulated since then. The literature shows both direct and indirect damaging effects of UV radiation (UVR, 280–400 nm) on almost all levels of the marine plankton community, with UVBR being one of the most harmful for aquatic organisms (2,3). Many of these studies focused on Antarctica, due to the presence of the so-called ozone hole. However, recent increases in ozone depletion in the Northern hemisphere (20–40%), related to combined effects of CFCs, climate warming and volcanic eruptions (4,5), focused interest on UVBR effects in other regions. Such studies predict that these factors acting together could result in a more severe ozone depletion in the Arctic than previously believed (4,5), similar to levels reported for Antarctica (~60%).

*Corresponding author email: gustavo_ferreyra@uqar.qc.ca (Gustavo A. Ferreyra)

Within this context, the lower Saint Lawrence Estuary area represents a midlatitude boreal region susceptible to ozone depletion (6).

Most of the previous experimental research on UVBR effects on aquatic organisms has been conducted using single taxon microcosm controlled experiments. These results are useful to define potential effects on specific targets and are essential for modeling processes, but are difficult to extrapolate to the natural environment. An alternative experimental approach is the use of outdoor mesocosms (containers >1 m^3; [7]), which are more representative of environmental physicochemical conditions. Several series of mesocosm experiments were performed in the lower Saint Lawrence Estuary during the last few years, and a wide range of results has been obtained. In general, vertical mixing in the mesocosms attenuated photoinhibition or damage by UVR (or both) as compared to fixed incubations at the surface (8). Nutrient kinetics were negatively affected by enhanced UVBR only under slow mixing regimes in the water column (9). Furthermore, surface incubation of phytoplankton preacclimated to mixing conditions in the mesocosms showed disparate results. Limited effects were found on phytoplankton photosynthetic activity and on the photosystem II (PSII)–associated D1 protein cycle under enhanced UVBR (8,10). Studies from the same community showed nonsynergistic effects of UVBR and some contaminants (polycyclic aromatic hydrocarbons) on both phytoplankton and bacteria, whereas others (tributylin) showed a synergic response, highlighting the importance of considering multiple stressors (11,12). Significant effects of enhanced UVBR on bacteria were also found in mesocosms with a natural plankton community of the St. Lawrence Estuary (13). The effects of UVBR were studied on bacteria, phytoplankton (two size classes) and protozooplankton (heterotrophic flagellates and ciliates) during the same experiment (14). The authors found a dramatic reduction in the abundance of large phytoplankton and ciliates. In turn, the decrease in ciliates resulted in a significant increase of their prey (*i.e.* bacteria, heterotrophic flagellates and small phytoplankton). Those authors (14) concluded that the community exposed to enhanced UVBR showed a trend toward a microbial food web (*i.e.* relative dominance of small microorganisms in relation to larger ones), instead of the more autotrophic herbivorous food web (15). These results highlight the importance of examining UVBR effects on the lower levels of the planktonic food web, because the observed changes may drastically reduce transfer of energy and matter toward higher trophic levels, as well as carbon export. In the context of carbon cycle dynamics in the ocean it is necessary to gain a more comprehensive understanding of the relative contribution of autotrophs and heterotrophs to carbon production and transfer. This information is essential for modeling future scenarios of global change and the biogeochemistry of the ocean. Therefore, the objective of this work was to simultaneously study the structure (composition and biomass) and processes (production) at the lower levels of a natural plankton community of the Saint Lawrence Estuary exposed to actual and enhanced UVBR, simulating worse ozone conditions (60% reduction), using outdoor mesocosms.

MATERIALS AND METHODS

Experimental design. The results presented in this paper are part of a larger study on the effects of enhanced UVBR on the lower levels of the plankton community. The experiment was performed 18–26 June 2000 at the south shore of the St. Lawrence Estuary (Rimouski, Quebec, Canada; 48.6°N, 68.2°W). A natural plankton community isolated from the lower St. Lawrence Estuary was exposed during 9 days to natural and enhanced levels of UVBR in clear mesocosms (2.3 m depth, 2000 L volume) immersed in the water column (see [13–15] for a detailed description of the structure of the mesocosms and experimental setup). Mesocosms were made of polyethylene transmitting 85–93% of light in the 280 to 750 nm wavelengths. These bags were attached to a wharf and filled simultaneously with water collected from a depth of 5 m off the coast of Rimouski 1 day prior to the start of the experiment. Large zooplankton were excluded by screening the water through 500 μm Nitex mesh. It has been shown that these organisms present avoidance responses to UVBR, and that their density decreases in surface waters during the hours of highest solar exposure (16). Consequently, this work focuses on the more exposed lower trophic levels of the community, which can evade harmful effects of UVBR only by passive vertical transport. To ensure a homogeneous distribution of organisms, the water column in the mesocosms was mixed continuously with Little Giant pumps (model 2-MD-HC) at a flow rate of 25 L min^{-1}.

The plankton community was exposed to two UVBR treatments: (1) natural UVBR (N), which was considered as the control treatment; and (2) natural plus enhanced UVBR (H), simulating 60% ozone depletion in the study area (17). Increased UVBR in the H treatment was supplied by four UVB fluorescent tubes (Philips TL40W-12RS, emission peak at 313 nm) positioned 40 cm above the water surface after preburning for 100 h. The tubes were covered with 0.13 mm cellulose diacetate sheets to screen out UV-C radiation (<280 nm) emitted by the lamps, and changed daily to avoid changes in spectral transmittance. Shading by the tube lamp holders in the N mesocosms was simulated by suspending wooden dummy lamps of the same size and position, which were placed at the same height from the water surface than the lamp holders. Fluorescent tube lamps were turned on daily from 1000 to 1500 h (see [17] for a detailed description of the lamps setup). Averaged 305 to 380 nm ratios for the period corresponding to the lamps turned on were 0.24 and 2.49 for the N and H treatments, respectively. Most of the days were sunny, with the exception of days 4 and 8, which were partially cloudy. Because lamps provided constant UV-B, potentially less DNA repair occurred during these days in the H treatment due to higher values in the above ratio (>4). Three replicate mesocosms were considered for each treatment. However, only data from two of the three N treatment replicates are shown in this paper, because the third one was excluded due to marked differences in the smaller cells detected by flow cytometry (two orders of magnitude higher than the other treatments from day 3), as well as in chlorophyll *a* (Chl *a*). Cells in the excluded mesocosm grew faster than in the other treatments and nutrients, particularly nitrate, and were exhausted more rapidly. This could be related to an input from surrounding waters into this mesocosm during the first days of the experiment, which changed the composition of the community as well as the nutrient load.

Light measurements. Incident UVR (305, 313, 320, 340 and 380 nm) and PAR were recorded every minute with a GUV-510 surface radiometer (Biospherical Instruments, Inc., San Diego, CA). Irradiance in the water column was measured three times every day (at 1000, 1230 and 1430 h local time) throughout the experiment with a PUV-542T profiling radiometer (Biospherical Instruments, Inc.) at the same wavelengths as incident UVR. Each set of profiles included two downcast and two upcast data records. Both instruments were intercalibrated after calibration by the manufacturer. Average daily incident light below the surface ($\bar{I}_0$, kJ m^{-2} nm^{-1}) and the vertical attenuation coefficient of light (K_d, m^{-1}) for UVR and PAR were calculated to estimate light penetration in the water column. $\bar{I}_0$ and K_d PAR, together with PAR incident irradiance, were used to calculate daily PAR in the water column of mesocosms. To describe the spectral light penetration in the water column we considered the depth of the photoactive zone (Z_{ph}, 10% of incident [18]), instead of the frequently used euphotic zone (Z_{eu}, 1% of incident). It was suggested that Z_{ph} is more representative of the potential degree of exposure of planktonic cells, because most of the photobiological processes take place through optical depths >10% of incident light at the water surface of the mesocosm (18).

Water column sampling and analyses. Daily sampling in the water column was performed between 0700 and 0730 h (local time) at 15–25 cm below the surface using the circulating pumps. Water samples were immediately transported to the laboratory in opaque polyethylene containers (20 L). At arrival at the laboratory (~15 min after sampling), subsamples were taken from the containers for analyses of nutrients (nitrate, nitrite, ammonia, phosphate and silicate), salinity, Chl *a*, particulate organic carbon and nitrogen (POC and PON, respectively), bacterial counts and activity, phytoplankton composition, abundance and photosynthesis, and microzooplankton identification and abundance. Water temperature in the

mesocosms was measured continuously with thermocouples (type "J") linked to a data logger (21X, Campbell Scientific, Inc., Edmonton, AB, Canada), and salinity was measured daily with an AutoSal salinometer (model 8400, Guildline Instruments, Inc., Lake Mary, FL).

Water subsamples (100 mL) for nutrient analyses (nitrate, nitrite, ammonia, phosphate and silicate) were filtered through precombusted Whatman GF/F filters and kept frozen (–80°C) until analyses with a Technicon IITM autoanalyzer system following the protocols described by the Joint Global Ocean Flux Study (19).

Subsamples (200 mL) were filtered onto precombusted Whatman GF/F filters and kept frozen (–20°C) until analysis of POC and PON with a Perkin-Elmer CHN analyzer (model 2400).

Bacteria. Water subsamples (10 mL) were filtered onto black polycarbonate membrane filters (Poretics; 0.2 μm pore size) for bacterial counts. Cells were stained with 4,6-diamidino-2-phenolindole (DAPI; Sigma Chemical Company, St. Louis, MO; 50 μg L^{-1} [20]), mounted onto slides and enumerated with a Zeiss epifluorescence microscope. To convert cell numbers to bacterial carbon biomass the factor of 20 fg C $bacterium^{-1}$ was used (14,21). Bacterial incorporation of ^{3}H-thymidine (^{3}H-TdR, Sigma; concentration 1.0 mCi mL^{-1} or 3.7×10^7 Bq mL^{-1}) was also measured (13,22). Three replicate 1.3 mL samples and two formaldehyde-killed controls (2% final concentration) were incubated at *in situ* temperature during 1 h, after addition of ^{3}H-TdR to a final concentration of 20 n*M*. Incubations were terminated by the addition of formaldehyde (2% final concentration) and extracted by microcentrifugation. Activity in the samples was measured using a Beckman LS 5801 scintillation counter. Rates of thymidine incorporation (total activity, TA; pmol ^{3}H-TdR L^{-1} h^{-1}) were calculated from DPM counts (22). TA was normalized to bacterial concentration to estimate cell-specific incorporation of thymidine (specific activity [SA]; fmol TdR $cell^{-1}$ h^{-1}). For the estimation of secondary bacterial production an empirical factor of 2×10^{18} cells produced per mole of ^{3}H-TdR was used, which represents the average of 97 studies (23,24).

Phytoplankton. Chl *a* concentration corrected for phaeopigments was measured fluorometrically according to the method described by the Joint Global Ocean Flux Study (25). One-hundred milliliter water subsamples were filtered onto Whatman GF/F filters immediately after arrival at the laboratory, followed by extraction with 100% acetone. Readings were performed with a Turner Designs fluorometer (model 10-005R) calibrated with standard Chl *a* (Sigma).

Phytoplankton <20 μm was enumerated by flow cytometry, whereas cells >20 μm were counted by optical microscopy. Two-hundred microliter subsamples were fixed with acid Lugol and kept in darkness at 4°C until further phytoplankton analysis. Cells were identified and measured for biovolume and cell carbon calculations using optical and scanning electron microscopy techniques (26,27). Phytoplankton enumeration was performed with an inverted microscope using the Utermöhl technique (28). Cell biovolume (μm^3) was calculated from cell measurements using the nearest matching geometric forms (29). Cell carbon estimations were made on the basis of calculated biovolumes (30).

Nanoplankton and picoplankton abundance was determined by flow cytometry. Duplicate 2 mL subsamples were analyzed immediately after arrival of mesocosm water samples to the laboratory with a FACSORT flow cytometer (FCM, Becton-Dickinson, NJ) equipped with a 488 nm laser. The flow rate was set to 60 μL min^{-1} and fluorescent beads (Polyscience Inc.) were used as an internal standard. Natural cellular fluorescence (red FL3, >650 nm, attributed to Chl *a*) was used to determine cell concentration (cells <20 μm). Data logging and analyses were performed using Becton-Dickinson Cell Quest and Attractor software programs, respectively.

To estimate carbon assimilation by phytoplankton, photosynthesis-irradiance relationships (*P-E*) were measured in each mesocosm (31). In dim light, a 13 mL subsample was poured into a 50 mL flask to which 13 μCi of $NaH^{14}CO_3^-$ was added (final activity of 37 KBq mL^{-1}). After a gentle homogenization, 1 mL aliquots were dispensed into 10 clean 20 mL borosilicate scintillation vials. The vials were then placed under a PAR gradient ranging from 6 to 800 μE m^{-2} s^{-1} in a linear incubator. These values were coincident with the PAR measurements performed in the water column of the mesocosms (maximum surface PAR observed at noon: ~700 μE m^{-2} s^{-1}). One scintillation vial was incubated in the dark. Total activity was determined by adding 50 μL of the inoculated water subsample into 10 mL of Fisherbrand ScintiVerse scintillation fluid containing 50 μL of 6 *N* NaOH. Nonincorporated ^{14}C was removed after 20 to 30 min of incubation by adding 500 μL of 6 *N* HCl. After 20 min, 500 μL of 6 *N* NaOH was added to the samples. Ten milliliters of scintillation cocktail was then added and the samples were counted using a Beckman LS 5801 scintillation counter. No photoinhibition was observed and hence the *P-E* relationships were fitted as described by the following equation (32):

$$P = P_m[1 - \exp(-\alpha E/P_m)] \quad (1)$$

where P (μg C L^{-1} h^{-1}) is the photosynthetic rate; P_m (μg C L^{-1} h^{-1}) is the maximum photosynthetic rate in the absence of photoinhibition; α (μg C L^{-1} h^{-1} [μE m^{-2} s^{-1}]$^{-1}$) is the initial slope of the photosynthetic light curve, which describes the photosynthetic efficiency and E (μE m^{-2} s^{-1}) represents the PAR. These parameters were used to estimate the daily integrated depth-average photosynthesis in the mesocosms. For doing this, every minute PAR at depths of 0.00, 0.25, 0.40, 0.75, 1.00 and 1.50 m was estimated from ambient GUV and PUV profiling measurements using the I_0 and K_d values obtained for each day. These values were introduced in the above equation as E, together with the corresponding photosynthetic parameters computed for each day. Daily photosynthesis was computed by time integration and water column averages of these integrated values were used for analysis.

Microzooplankton. To study microzooplankton composition and biomass, 250 mL samples were taken daily and preserved with acid Lugol (0.4% final concentration). Taxonomic identification (21,27,33), counts and measurements (length and diameter of all individuals in the analyzed subsamples) of loricae tintinnids and naked ciliates were made on 100 mL sedimented samples analyzed with an inverted microscope. Biovolumes were calculated as described for phytoplankton. Biovolumes of species were converted to biomass using a specific carbon ratio of $0.216 \times V^{0.939}$ (34).

Statistical analyses. Repeated-measures multivariate analysis of variance (MANOVA) was used to test for differences between treatments with Statistica 5.5 software. The primary constraint for MANOVA is that the difference between the number of samples (subjects) and the between-subjects treatment levels (groups) should be higher than the number of dependent variables (35). However, this condition is satisfied by the experimental design used in this study. Homogeneity of variances and normality were tested with Cochran C and Kolmogorov-Smirnov tests, respectively. Relationships between pairs of variables were fitted by model II regressions, because both dependent and independent variables were subjected to variability. Confidence intervals for the regressions were calculated (36). To test for the differences between treatments (categorical factors) controlling for continuous descriptors and dependent variables, a test of homogeneity of slopes was used (35). Then, a post hoc Tukey test was applied when significant differences between slopes were found.

RESULTS

UVBR exposure and temperature in the mesocosms

Light conditions were previously described in published papers from the same experiment (8,10–12). Consequently, here we report only complementary information. Z_{ph} for UVBR and UVAR (Z_{ph}^{UVBR} and Z_{ph}^{UVAR}) were ~0.5 and 1 m, respectively, and were above the maximum depth of the water column in the mesocosms (2.3 m; Fig. 1a). To compare with Z_{eu}, average UVBR and UVAR corresponding to the N treatment were added to Fig. 1, showing that only UVR in the 380 nm band reached the maximum depth in the mesocosms. In contrast, 10% PAR reached a depth of ~4 m, suggesting that cells were subjected to more variable UVR conditions than to PAR. The depth variability of Z_{ph}^{313} and Z_{ph}^{380} (corresponding here to 313 and 380 nm, respectively) is shown in Fig. 1b,c. A significant shallowing of these variables was observed from the start to the end of the experiment (~20%; $P < 0.01$). Significant differences between treatments were found only for Z_{ph}^{313}, and this from days 2 to 5 and for day 8 (Fig. 1b). During these days, Z_{ph}^{313} was deeper in N controls than in the H treatment.

Average temperature in the mesocosms for the entire experimental period was 11 ± 0.80°C (minimum = 9.0°C; maximum = 12.8°C), which was in the range of surface values typical of coastal waters in the area at the time of the study (www.osl.gc.ca/

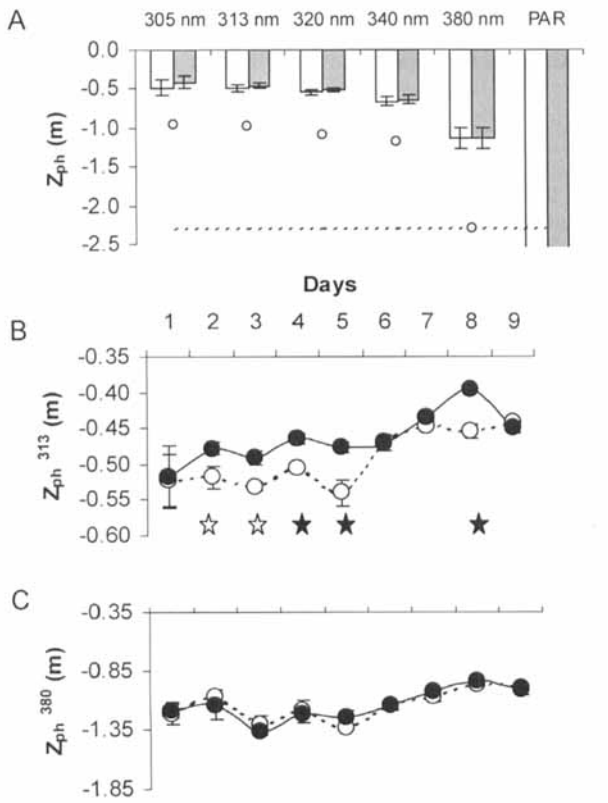

Figure 1. Photoactive zone depth (Z_{ph}, m) in the mesocosms. (a): Average of all data corresponding to the different UVR wavelengths measured and PAR for the N (natural UVBR, open bars) treatment and H (natural plus enhanced UVBR, grey bars) treatment. The dashed line represents the bottom depth of the mesocosms, and open circles correspond to the depth of the euphotic zone (Z_{eu}) for UVBR and UVAR in the N treatment. Vertical lines are standard deviations. (b and c): Daily variability of the photoactive zone depth (Z_{ph}, 10% incident light) corresponding to UVR irradiance at 313 and 380 nm within the N (open circles and dashed lines) and H (filled circles and continuous line) treatments, respectively. Open and filled stars denote significant differences between treatments at $P < 0.05$ and $P < 0.01$ probability levels, respectively. Vertical lines are standard deviations.

sl_monitore/en/data/st_riki.html). Salinity was nearly constant (~26) during the entire experiment.

Nutrients and total particulate organic material

Nutrient concentrations at the start of the experiment were ~15, 0.6, 1 and 19 μM for nitrate + nitrite, ammonium, phosphate and silicate, respectively. The initial molar N:P ratio was 15.5:1, which is similar to the expected Redfield ratio (16:1 [37]). These concentrations decreased sharply in all mesocosms during days 4 to 7, matching with the development of a phytoplankton bloom, until nearly total nutrient exhaustion (Fig. 2a–d). A lag was observed in the time at which the different nutrients reached exhaustion. Ammonium was the first to be consumed, reaching minimum concentrations at days 3–4 (Fig. 2b). Minimum concentrations of the other nutrients were observed from day 7, with silicate being consumed at a lower rate than nitrate and phosphate (Fig. 2d). To study the relation between external dissolved nitrogen and PON, the sum of nitrate, nitrite and ammonium was converted to $\mu g\ N\ L^{-1}$. Regression analysis shows that most of the initial external nitrogen ($195 \pm 16\ \mu g\ N\ L^{-1}$) was transferred to organic particles ($204 \pm 1\ \mu g\ N\ L^{-1}$) (Fig. 3). No significant differences were found between the slopes of H and control treatments ($P > 0.05$). POC increased from ~200 to 2500–3000 $\mu g\ L^{-1}$, and reached significantly higher values in the H treatment than in controls on days 8 and 9 (Fig. 4a; $P < 0.05$). This coincided with an increase in the particulate C:N ratio from ~5 to 15 between days 6 to 8 (data not shown). POC as a function of PON showed a linear relationship only until day 6 (Fig. 4b), which was also consistent with the relationship between POC and external nitrogen exhaustion (null values of external nitrogen corresponded to ~1000 $\mu g\ L^{-1}$ in POC; Fig. 4c).

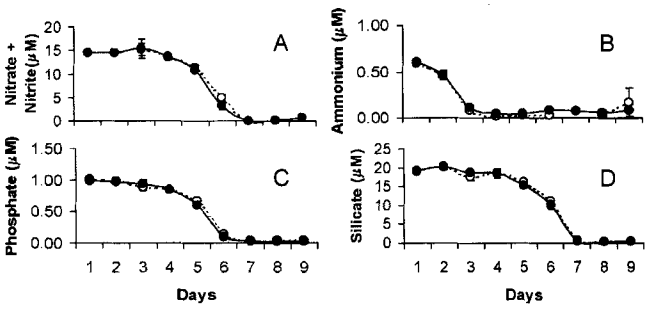

Figure 2. Daily variability in the concentration of nutrients (μM): (a) Nitrate + nitrite; (b) ammonia; (c) phosphate; (d) silicate. Open circles–dashed lines and filled circles–continuous lines correspond to the N (natural UVBR) and H (natural plus enhanced UVBR) treatments, respectively. Vertical lines are standard deviations.

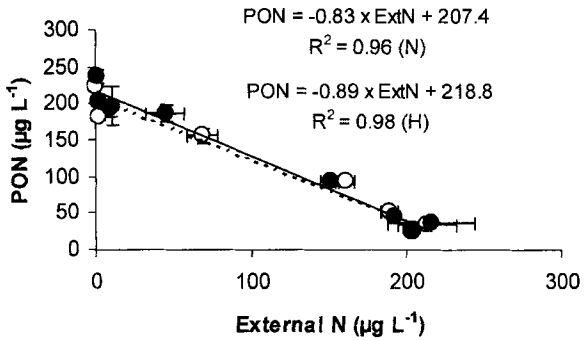

Figure 3. Particulate organic nitrogen ($\mu g\ L^{-1}$) as a function of external nitrogen concentration ($\mu g\ L^{-1}$): Open and filled circles correspond to the N (natural UVBR) and H (natural plus enhanced UVBR) treatments, respectively. Fitted regression lines (dashed and continuous for N and H treatments, respectively) were added to the figure, together with the corresponding equations and regression coefficients. Vertical and horizontal lines are standard deviations for both variables.

Plankton community dynamics

Phytoplankton abundance, composition, biomass and photosynthesis. The time series evolution of cell density showed three well-defined intervals: prebloom (days 1 to 3), bloom (days 4 to 7) and postbloom (days 7 to 9) (Fig. 5a). Flow cytometry results showed three phytoplankton size classes (1–3, 3–10 and 10–20 μm), which developed in the mesocosms during the experimental period. In this paper we considered the smaller fraction (1–3 μm) as picophytoplankton, and the sum of the 3–10 and 10–20 μm phytoplankton as nanophytoplankton. Phytoplankton >20 μm counted with the inverted microscope was categorized as microplankton. The nanophytoplankton fraction was the most abundant in this study, reaching maximum values of ~25×10^6 cells L^{-1}. This fraction represented 75–95% of total cell number during the bloom and postbloom periods, respectively. No significant differences were observed between treatments for each of the three size classes ($P > 0.05$).

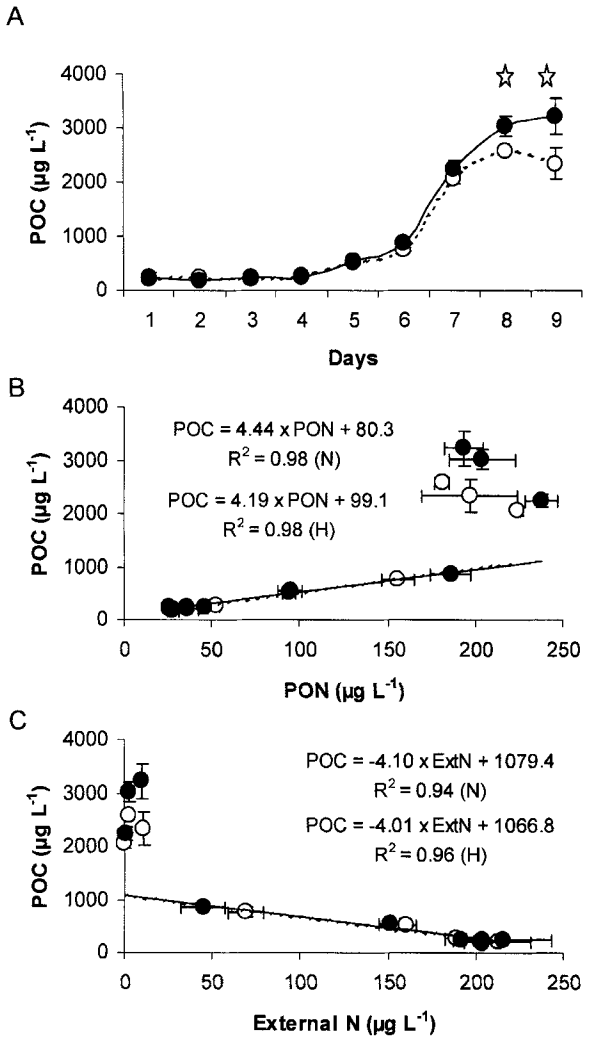

Figure 4. (a) Daily variability of particulate organic carbon (µg L^{-1}) in the mesocosms. Open circles–dashed lines and filled circles–continuous lines correspond to the N (natural UVBR) and H (natural plus enhanced UVBR) treatments, respectively. Open stars denote significant differences between treatments at the $P < 0.05$ level. (b) POC (µg L^{-1}) as a function of particulate organic nitrogen (µg L^{-1}) and (c) POC (µg L^{-1}) as a function of external nitrogen concentration (µg L^{-1}). Fitted regression lines (dashed and continuous for N and H treatments, respectively) corresponding to the first 6 days of the experiment were added to the figure, together with the corresponding equations and regression coefficients. Open and filled circles correspond to the N and H treatments, respectively. Vertical and horizontal lines are standard deviations for both variables.

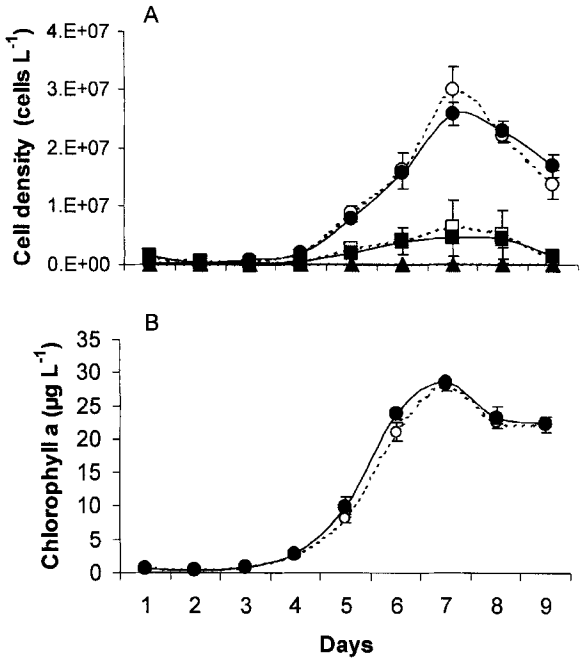

Figure 5. (a) Daily variability of phytoplankton cell density in the mesocosms (cell L^{-1}). Open symbols–dashed lines and filled symbols–continuous lines correspond to the N (natural UVBR) and H (natural plus enhanced UVBR) treatments, respectively. Squares, circles and triangles denote, respectively, the picophytoplankton, nanophytoplankton and microphytoplankton fractions identified by flow cytometry and optical microscopy. (b) Daily variability of chlorophyll *a* (µg L^{-1}) in the mesocosms. Open circles–dashed lines and filled circles–continuous lines correspond to the N and H treatments, respectively. Vertical lines are standard deviations.

Phytoplankton taxonomic composition was characterized by the presence of diatoms and phytoflagellates. A small *Chaetoceros* sp. (5–7 µm) was the most abundant diatom species, followed by *Thalassiosira pacifica* (10–20 µm) and *Chaetoceros diadema* (12–15 µm). Phytoflagellates were composed of Chlorophyta (*Chlamydomonas* sp.), Euglenophyta (*Eutreptia* sp. and *Euglenomorpha* sp.) and Prasinophyceae (*Pyramimonas* sp.).

Highest Chl *a* concentrations were reached on day 7 of the experiment (~30 µg Chl *a* L^{-1}), with the H treatment showing slightly higher but nonsignificant ($P > 0.05$) values during the exponential growth phase of the community (Fig. 5b). The different phytoplankton taxa were grouped within the size classes identified by flow cytometry for estimation of specific and total phytoplankton carbon concentration (TPC). The smaller size fractions determined by flow cytometry (*i.e.* 1–3 and 3–10 µm) were essentially constituted by small coccoid phytoflagellates and *Chaetoceros* sp. (5–7 µm), respectively. The 8–20 µm size fraction was composed primarily of *C. diadema, T. pacifica* and Chlorophyceae. Cells larger than 20 µm were primarily constituted by *T. pacifica* (35–50 µm, ~55%) and species from the family Eutreptiaceae (*Eutreptia* sp. and *Euglenomorpha* sp., ~38%). The major contribution to the phytoplankton carbon stock corresponded to the nanophytoplanktonic fraction (~90%). TPC showed a similar trend as Chl *a* throughout the experiment, presenting maximum values on day 7 (~1000 µg C L^{-1}) (Fig. 6a). TPC *vs* PON correlated positively ($R^2 = 0.94$ and $R^2 = 0.98$ for the N and H treatments, respectively), and no significant differences between treatments were found ($P > 0.05$) (Fig. 6b).

Carbon assimilation showed maximum values on day 7 (~400–500 µg C L^{-1} h^{-1}) in both treatments (Fig. 7). However, no significant differences between treatments were found during the time course of the experiment ($P > 0.05$).

Bacterial density, biomass and production. Part of the data from days 1 and 2 were lost, thus no statistical comparisons could be performed for these dates. Bacterial biomass gradually increased throughout the experiment until day 7 in the N treatment, and then decreased sharply on day 9 (Fig. 8a). The same trend was observed for the H treatment, but in this case the biomass decrease was delayed by 1 day. Maximum abundances observed were 1.5×10^9 and 2.2×10^9 cells L^{-1} on days 7 and 8 for the N and H treatments, respectively. The corresponding bacterial carbon values were ~30 and ~45 µg L^{-1}, respectively. Significant differences were observed only during the last 2 days of the experiment ($P < 0.05$), with higher bacterial biomass in the H treatment. Bacterial production, estimated from

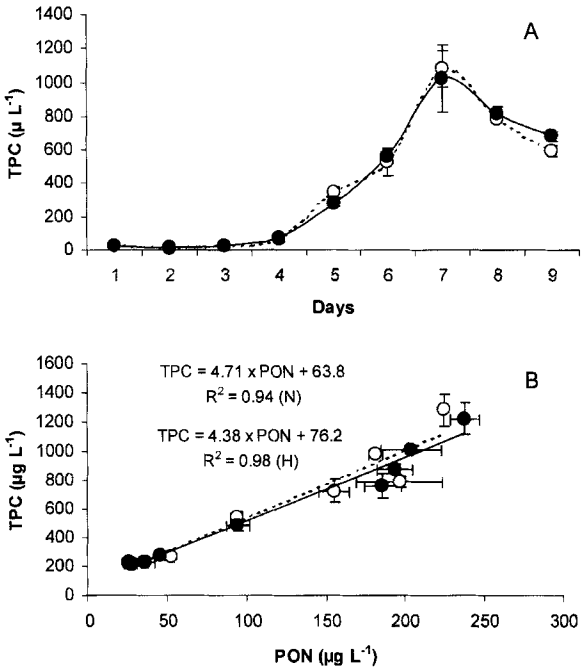

Figure 6. (a) Daily variability of total plankton carbon (µg L^{-1}) in the mesocosms. Open circles–dashed lines and filled circles–continuous lines correspond to the N (natural UVBR) and H (natural plus enhanced UVBR) treatments, respectively. Vertical lines are standard deviations. (b) TPC (µg L^{-1}) as a function of particulate organic nitrogen (µg L^{-1}). Open and filled circles correspond to the N and H treatments, respectively. Fitted regression lines (dashed and continuous for N and H treatments, respectively) were added to the figure, together with the corresponding equations and regression coefficients Vertical and horizontal lines are standard deviations for both variables.

TdR incorporation, varied between 0.5 and 1.5 µg C L^{-1} h^{-1} during most of the experiment, without differences between treatments (Fig. 8b). The only exception was day 9, when carbon incorporation was significantly higher in the H treatment. On the other hand, no significant differences were observed during any day for bacterial specific activity ($P < 0.05$; Fig. 8c).

Ciliate composition and biomass. Microzooplankton was essentially represented by ciliates (*Strombidinium* sp., *Tintinnopsis* sp., *Prorodon ovum*, *S. spiralis*, *Uronema marinum*, *Strombidinopsis* sp., *Ampidisca* sp. and *Lohmanniella oviformis*), and no other zooplankton categories could be observed with the methods used. The first three species were dominant in terms of biomass

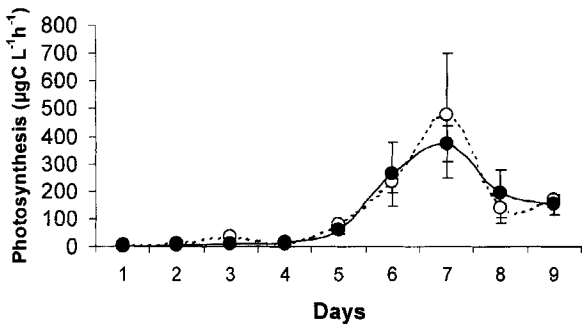

Figure 7. Daily variability of the average water-column photosynthesis in the mesocosms (µg C L^{-1} h^{-1}). Open circles–dashed lines and filled circles–continuous lines correspond to the N (natural UVBR) and H (natural plus enhanced UVBR) treatments, respectively. Vertical lines are standard deviations.

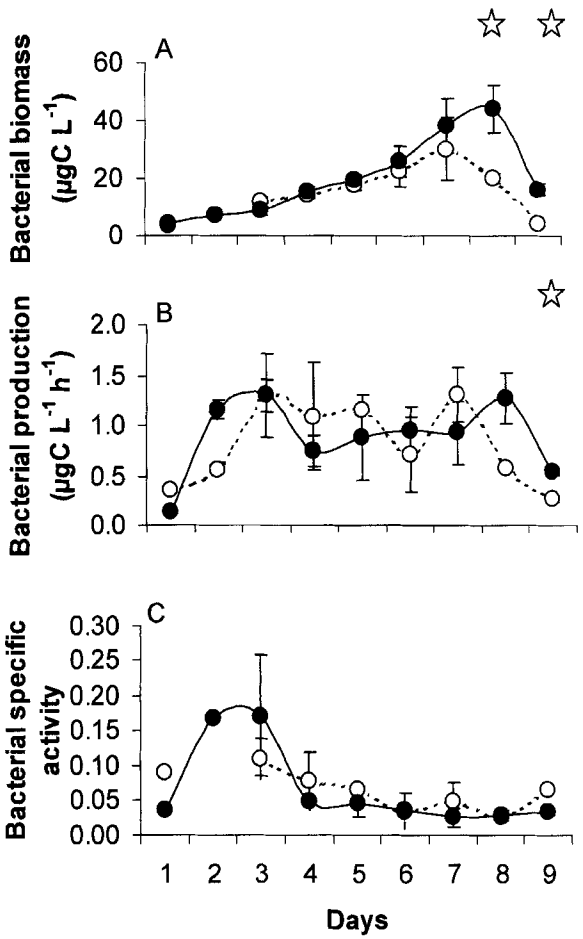

Figure 8. Daily variability of (a) bacterial cell carbon (µg C L^{-1}), (b) bacterial production (µg C L^{-1} h^{-1}) and (c) bacterial specific activity in the mesocosms. Open circles–dashed lines and filled circles–continuous lines correspond to the N (natural UVBR) and H (natural plus enhanced UVBR) treatments, respectively. Open stars denote significant differences between treatments at the $P < 0.05$ level. Vertical lines are standard deviations.

(>90%). Biovolumes corresponding to *Strombidinium* sp., *Tintinnopsis* sp., *P. ovum* and *S. spiralis* were 51 710, 56 968 and 41 888 μm^3, respectively. The biovolume of the remainder of the species identified ranged between 2000 and 20 000 μm^3. A significant ($P < 0.01$) lower total ciliate carbon biomass was observed in the H treatment, relative to the N controls, during the bloom and postbloom periods (by ~70% and 80% on days 5 and 9, respectively; Fig. 9). Significant changes were also observed in the abundance of the three dominant species. Carbon biomass was ~3–5 µg C L^{-1} on day 2 of the experiment, primarily from the contribution of *Strombidinium* sp. and *P. ovum* (>90% of total; Fig. 10a,b). The three species increased their biomass as a function of time in both treatments (Fig. 10a–c), with the exception of *Strombidinium* sp., which showed an inverse trend in the H treatment (Fig. 10a). On day 9, the biomass in the H treatment was significantly lower than that measured in the N one for the three species ($P < 0.05$ for *Strombidinium* sp. and $P < 0.01$ for *P. ovum* and *Tintinnopsis* sp., respectively). However, the percent of biomass reduction in the H treatment, relative to the N treatment, differed between these species. Whereas *Strombidinium* sp. and *Tintinnopsis* sp. presented ~90% reduction, such a value for *P. ovum* was much lower (~55%; Fig. 10a–c).

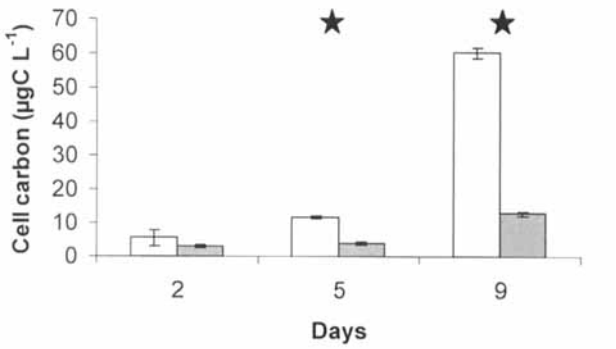

Figure 9. Ciliate biomass (µg C L^{-1}) in the mesocosms corresponding to the prebloom, bloom and postbloom periods (days 2, 5 and 9, respectively). Open and grey bars correspond to the N (natural UVBR) and H (natural plus enhanced UVBR) treatments, respectively. Filled stars denote significant differences between treatments at the $P < 0.01$ level. Vertical lines are standard deviations.

Food web carbon dynamics

The carbon dynamics for the different components of the studied system (*i.e.* phytoplankton, bacteria and microzooplankton) were analyzed in more detail. Only results from days 2, 5 and 9 were considered because simultaneous data on these components were available only for those dates. The dates chosen were representative of the prebloom, bloom and postbloom periods, respectively. In terms of biomass, the ratio of TPC to bacterial carbon (BC) showed a marked increase as a function of time, with maximum values at the end of the experiment (Fig. 11a). This ratio was significantly higher in the N treatment than in the H treatment during the bloom and postbloom periods ($P < 0.05$ and $P < 0.01$, respectively). In terms of production rates, the ratio of phytoplankton *vs* bacterial production showed a trend similar to their respective biomass carbon ratio, but in this case significant differences between treatments (N > H; $P < 0.05$) were found only during the postbloom period (Fig. 11b). The same temporal trend was shown by the TPC *vs* total bacterial and ciliate carbon (TBCC) ratio (Fig. 11c). However, this ratio showed maximum values in the H treatment ($P < 0.01$) during the postbloom period in contrast to the TPC:BC ratio (due to the strong decrease in ciliate carbon in the H treatment).

As shown above for the POC:PON ratio, the POC:TPC ratio correlated linearly only until day 6 (Fig. 12), without significant correlations between these variables for the postbloom period. A similar trend was observed for the POC:Chl *a* ratio (data not shown). Regression estimated POC concentrations corresponding to null Chl *a* and TPC concentration were ~200 µg POC L^{-1}, indicating the initial contribution of nonautotrophic carbon.

Considering days 2, 5 and 9, the differences observed during the postbloom also apply for the ratio of POC:TCC (TCC represents total community carbon, or the sum of autotrophic plus heterotrophic carbon; Fig. 13). On day 9, the heterotrophs contribution to TCC in N and H was only ~10% and 4%, respectively. Consequently, most of the contribution to TCC came from phytoplankton. However, as shown in Fig. 13, POC was ~3.5 and ~4.5 times higher than calculated TCC in the N and H treatments, respectively, at that date.

DISCUSSION

Plankton production and biomass

Initial nutrient concentrations in the mesocosms were within the ranges observed for the lower St. Lawrence Estuary during the prebloom period (38). These conditions allowed the development of a high phytoplankton biomass stock, with external nitrogen totally converted to biomass. As a result, Chl *a* values reached were close to the maximum reported for the area during summer (38).

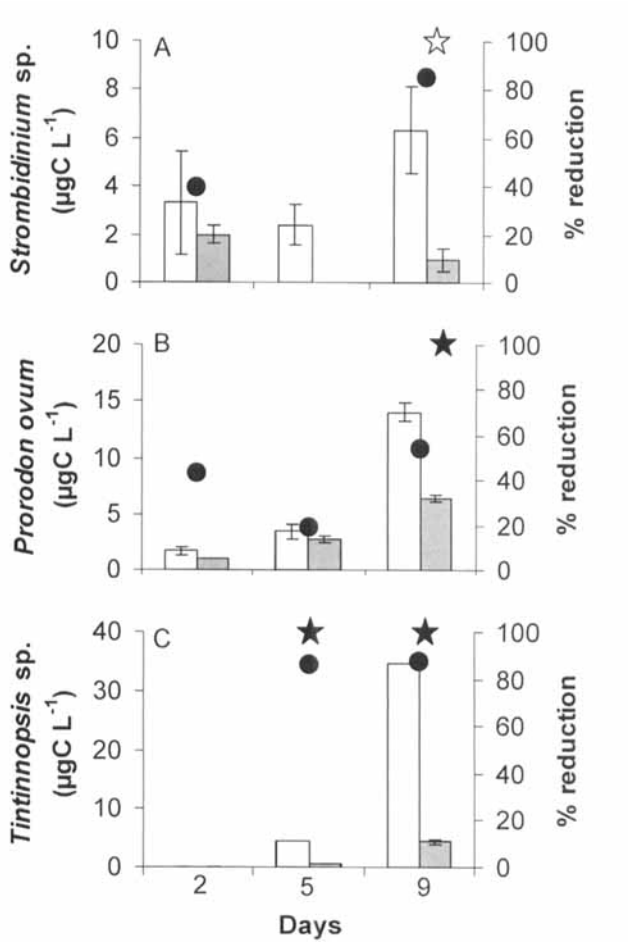

Figure 10. Biomass of dominant ciliate species (%) in the mesocosms corresponding to the prebloom, bloom and postbloom periods (days 2, 5 and 9, respectively). (a) *Strombidinium* sp., (b) *Prorodon ovum* and (c) *Tintinnopsis* sp. Open and grey bars are N (natural UVBR) and H (natural plus enhanced UVBR) treatments, respectively. Open and filled stars denote significant differences between treatments at $P < 0.05$ and $P < 0.01$ probability levels, respectively. Vertical lines are standard deviations. The right scale–filled circles indicate the percent of reduction of biomass in the H treatment relative to controls for the different species.

Phytoplankton abundance changed markedly as a function of time, with nanophytoplankton being the dominant fraction during the entire study. However, no significant differences were observed between treatments for the different size fractions identified, nor for TPC, Chl *a* and photosynthesis. Photosynthesis results are consistent with published information from the same experiment on the combined effect of nutrient stress and UVBR on the phytoplankton community (8). Those authors found significant physiological effects only on the PSII system under nutrient stress conditions (*i.e.* during the postbloom period). However, their results are from surface incubations, which excluded the alleviation of UVBR effects by vertical mixing in the water column of the mesocosms. Mixing plays an important role in modulating the effects of UVBR on phytoplankton physiology and nutrient dynamics, as reported from field and laboratory vertical mixing simulations (9,39). Furthermore, results from studies performed simultaneously with ours on the dynamics of the D1 protein cycle, involved in the repair of PSII,

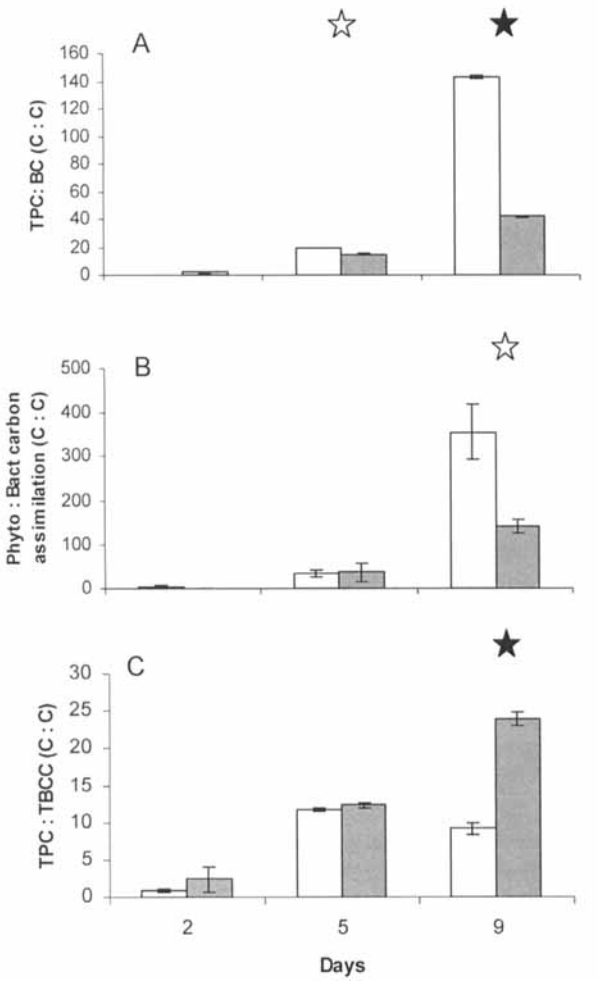

Figure 11. (a) TPC:BC (total phytoplankton carbon to bacterial carbon), (b) phytoplankton:bacterial carbon assimilation and (c) TPC:TBCC (total phytoplankton carbon to total bacteria and ciliate carbon) ratios. Open and grey bars are N (natural UVBR) and H (natural plus enhanced UVBR) treatments, respectively. Open and filled stars denote significant differences between treatments at the $P < 0.05$ and $P < 0.01$ levels, respectively. Vertical lines are standard deviations.

showed a lack of effect of the UVBR treatments on the quantum yield of PSII photochemistry (F_v/F_m) (10). Consequently, we suggest that the combined dynamics of mixing and photoprotection allowed phytoplankton to cope with harmful effects of UVBR.

According to the continuum trophic pathways hypothesis (15), microzooplankton plays a key role in carbon transfer in pelagic food webs. It represents a link between small phytoplankton and bacterial production (*i.e.* via grazing [40]) and higher trophic levels (*i.e.* via metazoan predation [41]). Biomass of ciliates at the start of the experiment was consistent with data reported for May–September in the lower St. Lawrence Estuary (11.17 ± 11.19 μg C L^{-1} [21]). This component of the system was strongly affected by UVBR, not only in terms of biomass but also in relative abundance. This suggests that periodic excursion below Z_{ph}^{UVBR} was not enough to allow repair of damaged targets in the cells. The observed 70–80% lower ciliate carbon biomass observed in the H treatment (see Fig. 9) was consistent with previous results (14), with 64% reduction under enhanced UVBR in a similar mesocosms experiment with water from the St. Lawrence Estuary. *P. ovum* was the most resistant species, compared with that of the other numerically dominant species (*Strombidinium* sp. and

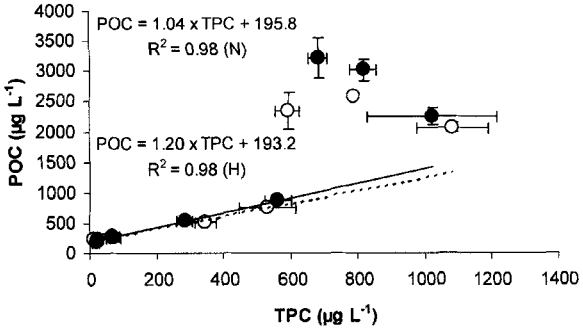

Figure 12. Particulate organic carbon (μg L^{-1}) as a function of total phytoplankton carbon (μg L^{-1}): Open and filled circles correspond to the N (natural UVBR) and H (natural plus enhanced UVBR) treatments, respectively. Fitted regression lines (dashed and continuous for N and H treatments, respectively) corresponding to the first 6 days of the experiment were added to the figure, together with the corresponding equations and regression coefficients. Vertical and horizontal lines are standard deviations for both variables.

Tintinnopsis sp.), showing that enhanced UVBR can significantly alter community composition, and probably trophic relationships and carbon pathways. Other studies have shown negative and positive responses of various microzooplankton species to UVBR enhancement (42), indicating the absence of a general pattern for such responses. However, our results support previous results that suggest that the ciliate community of the St. Lawrence Estuary is highly sensitive to enhanced UVBR (14).

Together with microzooplankton, bacteria play a central role in the planktonic food web as a link between DOC and energy transfer toward higher trophic levels. Moreover, it has been suggested that probably most of the respiration in the ocean comes from bacteria (43). Bacterial abundance ($\sim 1 \times 10^9 \pm 0.6 \times 10^9$ cell L^{-1}) and carbon concentrations ($\sim$19.8 ± 13.9 μg C L^{-1}) in this experiment were within the ranges reported for the lower St. Lawrence Estuary (21). A continuous increase in bacterial biomass was observed, following the evolution of phytoplankton concentration, with a sharp bacterial decrease at the end of the experiment under both treatments. The latter could be related to nutrient limitation, as observed during a similar experiment (13).

Changes in the composition or relative abundance of the different bacterial species could not be evaluated by the methods used here. Despite this limitation, general information about the responses of this group can be inferred. Bacterial production rates did not show direct UVBR effects, as suggested by the lack of differences between treatments observed in carbon-specific activity. This could be explained by internal and external alleviating mechanisms (*i.e.* repair of UVBR damaged targets and mixing, respectively), or by changes in the composition of the community from less to more resistant species. Another explanation for the lack of differences between UVR treatments may be the balance between harmful direct effects and increases in respiring substrates due to UVBR-enhanced photolysis of high molecular weight DOC (13,44). Consequently, the significant bacterial biomass increase observed during the postbloom period in the H treatment relative to controls are not attributed to differential bacterial growth but was probably caused by a decrease in grazing pressure due to a slower growth rate or to a high mortality of ciliates, or both.

Carbon partition within the community

Both the ratio of phytoplankton to bacterial carbon biomass and production (Fig. 11a,b) showed significant lower values in the H

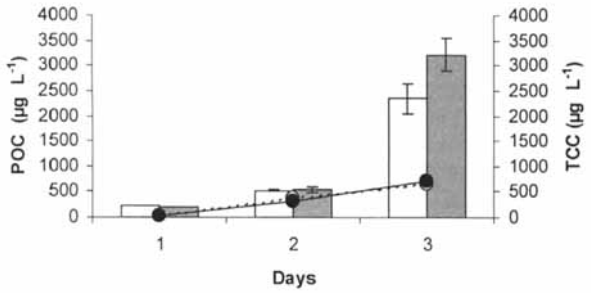

Figure 13. Particulate organic carbon (vertical bars, µg C L^{-1}) and total community carbon (circles and lines) in the mesocosms corresponding to the prebloom, bloom and postbloom periods (days 2, 5 and 9, respectively). Open circles–dashed lines and open bars correspond to the N (natural UVBR) treatment, whereas filled circles–continuous lines and grey bars denote the H (natural plus enhanced UVBR) treatment. Vertical lines are standard deviations.

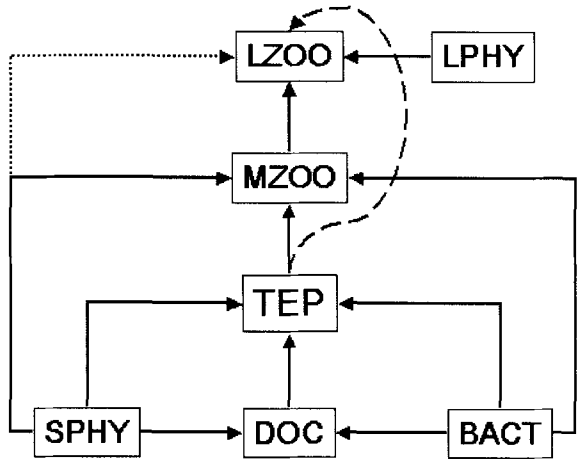

Figure 14. Diagram representing the transparent exopolymer particle (TEP) hypothesis. The arrows represent transfer of matter between the different compartments. Small phytoplankton cells (SPHY) and bacteria (BACT) release dissolved organic carbon (DOC). These cells are in part aggregated into TEP. Both SPHY and BACT are preyed on directly by microzooplankton (MZOO) and indirectly by inclusion of cells in TEP. Large zooplankton (LZOO) directly preys on both MZOO and large phytoplankton cells (LPHY). Grazing by LZOO on SPHY was considered less significant (dotted arrow) than the other transfer processes. LZOO can directly feed on TEP, bypassing the microbial loop (curved arrow).

treatment at the end of the experiment. These observations are in line with previous findings (14,45), which reported that the plankton community can evolve toward a microbial food web under enhanced UVBR conditions. However, these authors reported 35% reduction in the TPC:BC ratio under such conditions, instead of the 71% found in our experiment. On the other hand, the TPC:TBCC ratio showed higher values in the H than in the N treatment on day 9 (Fig. 11c), contrasting with their results (20% reduction in the H treatment for the TPC:TBCC ratio). This can be explained by the strong reduction of the ciliate biomass under the H treatment, which was more intense in our experiment (83% reduction instead of 64% reduction [14]), combined with the lack of change in TPC. Consequently, these results strengthen the idea that enhanced UVBR can alter the dynamics and structure of the lower trophic levels of the plankton community, as well as the potential carbon transfer toward metazoan predators, which can be significantly reduced under these conditions.

It is interesting to note the sharp increase in POC during the postbloom period, which resulted in the lack of a linear relationship between POC and other variables (PON, external nitrogen evolution, Chl *a* and TPC; Figs. 4bc and 12a,b, respectively). Cell secretion of organic matter could contribute to explain these results. Phytoplankton secretion of energy-rich substances represents 5–25% of carbon fixed into particulate matter, and is released at constant proportions of photosynthetic rates by healthy cells (46). Furthermore, it has been shown that extracellular carbon produced by phytoplankton can be increased significantly by the uncoupling between nutrients and light availability (47–49). Mechanisms controlling this process remain unclear, but there is evidence that under inorganic nutrient limitation and high light conditions photosynthetic products cannot be efficiently channeled to growth. Consequently, a fraction of dissolved inorganic carbon uptake by photosynthesis is "overspilled" via the production of low nitrogen compounds, which are released by cells to the water column (50). Some of these compounds are acidic sugars that facilitate aggregation into >0.7 µm particles known as total exopolymer particles (TEPs; [51,52]), which may constitute a significant fraction of POC (53). This is consistent with the suggestion that a significant fraction of the DOC pool in the ocean presents a dynamic dispersion/assembly process of these particles, which can reach 6–8 µm (54). These processes are represented in the diagram in Fig. 14.

In our experiment TPC was ~1000 µg L^{-1} at the onset of nutrient limitation, similar to the POC concentration at that moment. Thereafter, POC increased by ~60% in both treatments, which is in the range of reported increments (~35–69% [55,56]). It has been shown that volume-derived carbon estimations are not accurate under conditions of nutrient exhaustion (57). The authors performed two mesocosm studies with different Si:N ratios (1:1 and 4:1) at the start of the experiments. Roughly, a ~40% underestimation of POC can be derived from their figures, considering their results corresponding to the Si:N ratio of 1:1, which was similar to the initial conditions in our experiment. Even assuming this strong difference and correcting the TPC fraction of the estimated TCC shown in Fig. 13, measured POC was significantly higher than TCC on day 9 (increase from 650 to 890 and from 700 to 980 µg C L^{-1} in the N and H treatments, respectively). Most of the large differences found in this work between TCC and POC during the postbloom period (Fig. 13) may be explained by a significant TEP contribution to total POC following nutrient exhaustion. However, this interpretation cannot explain the significant differences between treatments observed in POC concentration. It has been suggested that enhanced UVBR may play a role in increasing extracellular excretion (46), but no direct effects have been reported up to now.

Furthermore, experimental results show that UVBR hinders the exchange between DOC and the gel phase in the ocean by inhibiting the spontaneous assembly of polymers, by cleaving DOC or by dispersing assembled gel particles (or both) (58). Consequently, there is an apparent contradiction between these results and the higher POC concentrations observed during this study in the H treatment compared to the N treatment. Assuming that the TEP input to total POC hypothesis presented here is correct (see Fig. 14), we suggest that the differences between treatments observed in POC concentration may be attributed to a strong decrease in ciliate TEP ingestion, in coincidence with an increased extracellular release under enhanced UVBR and nutrient limitation. Under this proposed scenario, UVBR would significantly modify the carbon pathway in the water column.

It has been shown that TEPs can be used as a direct energy source for both bacteria and zooplankton and play a significant role structuring the ciliate community (59). Moreover, the aggregation of small particles into larger ones makes them available to larger zooplankton such as euphasiids, thus playing a significant role in carbon transfer toward higher trophic levels (60). Large herbivores such as krill can feed directly on nanophytoplankton and picophytoplankton included in TEP particles, thus bypassing the microbial loop (61) (Fig. 14). Assuming that UVBR has minor effects on large zooplankton due to avoidance, TEPs may result in an enhanced transfer of carbon toward higher trophic levels through this pathway. Consequently, a UVBR-induced TEP increase under nutrient-limiting conditions may be interpreted as relatively advantageous for carbon transfer within the planktonic food web, in the sense that energy is not completely lost for the pelagic system and that a significant fraction can be returned back to the planktonic food web system.

The potential synthesis of TEPs and DOC release during prebloom conditions in our experiment could also contribute to explaining the differences in light transmission between treatments observed in Z_{ph}^{UVBR} between days 2–5. This is consistent with mesocosm experimental results that showed that these particles are also synthesized before the onset of the bloom (62). Furthermore, an additional contribution to the relatively high UVBR absorption in the H treatment could be the release of mycosporine-like amino acids (MAAs). It has been suggested that these substances may contribute to the reduction of UVR transmission through the water column (3,63). However, data on DOC and MAAs were not available for this work.

Models predict a shallowing of the upper mixed layer and a reduced vertical exchange of nutrients in the ocean due to the global rise in temperature (64,65). A shallower, upper mixed layer could increase the residence time of cells in the surface layer, and hence augment exposure to UVBR (38). Under such a scenario, the proposed UVBR-TEP–related processes described above may become significant in modifying the carbon cycle in the ocean, which is a most important research subject because of global warming. Our results suggest the importance of measuring TEPs and DOC in future experiments to study the effects of UVBR on plankton communities.

Acknowledgements—This work was supported by Inter American Institute for Global Change Research (IAI) grant CRN-26 and by a team grant from the Natural Sciences and Engineering Research Council of Canada (NSERC) to S.D., and by individual NSERC grants to S.D. and S.R. We sincerely thank Karine Lacoste for her efficient coordination in the organization and deployment of this experiment, Aurore Trottet for ciliate identification and counts and Sebastien Mas and Gervais Ouellet for helping in cytometric analysis and photosynthesis experiments. We also acknowledge the helpful criticisms and useful comments on the manuscript by Claude Belzile.

REFERENCES

1. Whitehead, R. F., S. J. de Mora and S. Demers (2000) Enhanced UV radiation—A new problem for the marine environment. In *The Effects of UV Radiation in the Marine Environment* (Edited by S. J. de Mora, S. Demers and M. Vernet), pp. 1–34. Cambridge University Press, Cambridge, UK.
2. Vincent, W. F. and S. Roy (1993) Solar ultraviolet-B radiation and aquatic primary production: Damage, protection and recovery. *Environ. Rev.* **1**, 1–12.
3. Perin, S. and D. R. S. Lean (2004) The effects of ultraviolet-B radiation on freshwater ecosystems of the Arctic: Influence from stratospheric ozone depletion and climate change. *Environ. Rev.* **12**, 1–70.
4. Shindell, D. T., D. Rind and P. Lonergan (1998) Increased polar stratospheric ozone losses and delayed eventual recovery owing to increasing greenhouse-gas concentrations. *Nature* **392**, 589–592.
5. Tabazadeh, A., K. Drdla, M. R. Schoeberl, P. Hamill and O. B. Toon (2002) Arctic "ozone hole" in a cold volcanic stratosphere. *Proc. Natl. Acad. Sci. U. S. A.* **99**, 2609–2612.
6. Scientific assessment of ozone depletion: 2002 (2003) World Meteorological Organization—Global ozone research and monitoring project—report no. 47. Geneva. Available at: www.wmo.ch/web/arep/reports/o3_assess_rep_2002_front_page.html. Accessed 20 June 2006.
7. Guanguo, L. (1990) Different types of ecosystem experiments. In *Enclosed Experimental Marine Ecosystems: A Review and Recommendations* (Edited by C. M. Lalli), pp. 7–19. Coastal and Estuarine Studies, Springer-Verlag, New York.
8. Longhi, M. L., G. A. Ferreyra, I. Schloss and S. Roy (2005) Variable phytoplankton response to enhanced UV-B and nitrate addition in mesocosm experiments at three latitudes (Canada, Brazil and Argentina). *Mar. Ecol. Prog. Ser.* **313**, 57–72.
9. Fouilland, E., M. Gosselin, B. Mostajir, M. Levasseur, J.-P. Chanut, S. Demers and S. de Mora (2003) Effects of ultraviolet-B radiation and vertical mixing on nitrogen uptake by a natural planktonic community shifting from nitrate to silicic acid deficiency. *Limnol. Oceanogr.* **48**, 18–30.
10. Bouchard, J. N., D. A. Campbell and S. Roy (2005) Effects of UV-B radiation on the D1 protein repair cycle of natural phytoplankton communities from three latitudes (Canada, Brazil, and Argentina). *J. Phycol.* **41**, 273–286.
11. Sargian, P., B. Mostajir, K. Chatila, G. A. Ferreyra, É. Pelletier and S. Demers (2005) Non-synergistic effects of water-soluble crude oil and enhanced ultraviolet-B radiation on a natural plankton assemblage. *Mar. Ecol. Prog. Ser.* **249**, 63–77.
12. Sargian, P., É. Pelletier, B. Mostajir, G. A. Ferreyra and S. Demers (2005) TBT toxicity on a natural planktonic assemblage exposed to enhanced ultraviolet-B radiation. *Aquat. Toxicol.* **73**, 299–314.
13. Chatila, K., S. Demers, B. Mostajir, M. Gosselin, J.-P. Chanut, P. Montfort and D. Bird (2001) The response of natural bacterioplankton community to different levels of ultraviolet-B radiation: A food web perspective. *Microb. Ecol.* **41**, 56–68.
14. Mostajir, B., S. Demers, S. de Mora, C. Belzile, J.-P. Chanut, M. Gosselin, S. Roy, P. Z. Villegas, J. Fauchot, J. Bouchard, D. Bird, P. Monfort and M. Levasseur (1999) Experimental test of the effect of ultraviolet-B radiation in a planktonic community. *Limnol. Oceanogr.* **44**, 586–596.
15. Legendre, L. and F. Rassoulzadegan (1995) Plankton and nutrient dynamics in marine waters. *Ophelia* **41**, 153–172.
16. Alonso, C., V. Rocco, J. P. Barriga, M. A. Battini and H. Zagarese (2004) Surface avoidance by freshwater zooplankton: Field evidence on the role of ultraviolet radiation. *Limnol. Oceanogr.* **49**(1), 225–232.
17. Díaz, S., C. Camilión, J. Escobar, G. Deferrari, S. Roy, K. Lacoste, S. Demers, C. Belzile, G. Ferreyra, S. Gianesella, M. Gosselin, C. Nozais, E. Pelletier, I. Schloss and M. Vernet (2006) Simulation of ozone depletion using ambient irradiance supplemented with UV lamps. *Photochem. Photobiol.* **82**, 857–864.
18. Neale, P. J., E. W. Helbling and H. E. Zagarese (2003) Modulation of UVR exposure and effects by vertical mixing and advection. In *UV Effects in Aquatic Organisms and Ecosystems* (Edited by E. W. Helbling and H. Zagarese), pp. 107–134. The Royal Society of Chemistry, Cambridge, UK.
19. Joint Global Ocean Flux Study (JGOFS) protocols (Chapter 9–12). Available at: http://www.pangaea.de/Projects/JGOFS/Methods. Accessed on 1 May 2006.
20. Porter, K. G. and Y. S. Feig (1980) The use of DAPI for identifying and counting aquatic microflora. *Limnol. Oceanogr.* **25**, 943–948.
21. Sime-Ngando, T., M. Gosselin, S. Roy and J.-P. Chanut (1995) Significance of planktonic ciliated protozoa in the Lower St. Lawrence Estuary: Comparison with bacterial, phytoplankton, and particulate organic carbon. *Aquat. Microb. Ecol.* **9**, 243–258.
22. Fuhrman, J. A. and F. Azam (1982) Thymidine incorporation as a measure of heterotrophic bacterioplankton production in marine surface waters: Evaluation and field results. *Mar. Biol.* **66**, 109–120.
23. Ducklow, H. W. and C. A. Carlson (1992) Oceanic bacterial production. *Adv. Microb. Ecol.* **12**, 113–181.

24. Chin-Leo, G. (2002) Bacterial secondary productivity. In *Manual of Environmental Microbiology* (Edited by C. J. Hurst, R. L. Crawford, G. R. Knudsen, M. J. McInerney and L. D. Stetzenbach), pp. 354–363. American Society for Microbiology Press, Washington, DC.
25. Joint Global Ocean Flux Study (JGOFS) protocols. Chapter 14. Available at: http://www.pangaea.de/Projects/JGOFS/Methods. Accessed on 1 May 2006.
26. Ferrario, M. E., E. Sar and S. Sala (1995) Metodología básica para el estudio del fitoplancton con espacial referencia a las diatomeas. In *Manual de Métodos Ficológicos* (Edited by K. Alveal, M. E. Ferrario, E. C. Oliveira and E. Sar), pp. 1–23. Universidad de Concepción, Editora A. Pinto, Chile.
27. Bérard-Therriault, L. (1999) Guide d'identification du phytoplancton marin de l'estuaire et du golfe du Saint-Laurent incluant également certains protozoaires. Presses scientifiques du CNRC, Ottawa.
28. Lund, J. W. G., C. Kipling and E. D. Le Cren. (1958) The inverted microscope method of estimating algal numbers and the statistical basis of estimations by counting. *Hydrobiologia* **11**, 143–170.
29. Hillebrand, H., C.-D. Dürselen, D. Kirschtel, U. Pollingher and T. Zohary (1999) Biovolume calculation for pelagic and benthic microalgae. *J. Phycol.* **35**, 403–424.
30. Verity, P. G., C. Y. Robertson, C. R. Tronzo, M. G. Andrews, J. R. Nelson and M. E. Sieracki (1992) Relationships between cell volume and the carbon and nitrogen content of marine photosynthetic nanoplankton. *Limnol. Oceanogr.* **37**, 1434–1446.
31. Lewis, M. R. and J. C. Smith (1983) A small volume, short-incubation-time method for measurement of photosynthesis as a function of incident irradiance. *Mar. Ecol. Prog. Ser.* **13**, 99–102.
32. Platt, T., C. L. Gallegos and W. G. Harrison (1980) Photoinhibition of photosynthesis in natural assemblages of marine phytoplankton. *J. Mar. Res.* **38**, 687–701.
33. Lee, J. J. (2000) *An Illustrated Guide to the Protozoa.* Society of Protozoologists, Allen Press, Inc., Lawrence, Kansas.
34. Menden-Deuer, S. and E. J. Lessard (2000) Carbon to volume relationships for dinoflagellates, diatoms, and other protist plankton. *Limnol. Oceanogr.* **45**, 569–579.
35. Scheiner, S. M. and J. Gurevitch (2001) *Design and Analysis of Ecological Experiments* 2nd ed. Oxford University Press, New York.
36. Ricker, W. E. (1973) Linear regression in fishery research. *J. Fish. Res. Board. Can.* **30**, 409–434.
37. Redfield, A. C., B. H. Ketchum and F. A. Richards (1963) The influence of organisms on the composition of seawater. In *The Sea*, Vol. 2 (Edited by M. N. Hill), pp. 26–79. Wiley Interscience, New York.
38. Starr, M., L. St-Amand and L. Bérard-Therriault (2002) State of phytoplankton in the Estuary and Gulf of St. Lawrence during 2001. Research Document 2002/067, pp. 1–22. Canadian Science Advisory Secretariat, Maurice Lamontagne Institute, Mont Joli, Quebec Fisheries and Oceans Canada.
39. Hernando, M. P. and G. A. Ferreyra (2005) The effects of UV radiation on photosynthesis in an Antarctic diatom (*Thalassiosira* sp.): Does vertical mixing matter? *J. Exp. Mar. Biol. Ecol.* **325**, 35–45.
40. Sakka, A., L. Legendre, M. Gosselin and B. Delesalle (2000) Structure of the oligotrophic planktonic food web under low grazing of heterotrophic bacteria: Takapoto Atoll, French Polynesia. *Mar. Ecol. Prog. Ser.* **197**, 1–17.
41. Nakano, S.-I. (2000) The role of protists in microbial loop of lake ecosystems. *Jpn. J. Ecol.* **50**, 41–54.
42. Davidson, A. and L. Belbin (2002) Exposure of natural Antarctic marine microbial assemblages to ambient UV radiation: Effects on the marine microbial community. *Aquat. Microb. Ecol.* **27**, 159–174.
43. Karl, D. M., E. A. Laws, P. Morris, P. J. le B. Williams and S. Emerson (2003) Metabolic balance of the open sea. *Nature* **426**, 32.
44. Lindell, M. J., H. W. Granéli and L. J. Tranvik (1995) Enhanced bacterial response to photochemical transformation of dissolved organic matter. *Limnol. Oceanogr.* **40**, 195–199.
45. Mostajir, B., S. Demers, S. J. de Mora, R. P. Bukata and J. Jerome (2000) Implications of UV radiation for the food web structure and consequences on the carbon flow. In *The Effects of UV Radiation in the Marine Environment* (Edited by S. de Mora, S. Demers and M. Vernet), pp. 310–320. Cambridge University Press, Cambridge, UK.
46. Vernet, M. (2000) Effects of UV radiation on the physiology and ecology of marine phytoplankton. In *The Effects of UV Radiation in the Marine Environment* (Edited by S. de Mora, S. Demers and M. Vernet), pp. 237–278. Cambridge University Press, Cambridge, UK.
47. Myklestad, S. and A. Haug (1972) Production of carbohydrates by the marine diatom *Chaetoceros affinis* var. *Willei* (Gran) Hustedt. I. Effect of the concentration of nutrients in the culture medium. *J. Exp. Mar. Biol. Ecol.* **9**, 125–136.
48. Wood, A. M. and L. M. Van Valen (1990) Paradox lost? On the release of energy-rich compounds by phytoplankton. *Mar. Microb. Food Webs* **4**, 103–116.
49. Norrman, B., L. Zweifel, C. S. J. Hopkinson and B. Fry (1995) Production and utilization of dissolved organic carbon during an experimental diatom bloom. *Limnol. Oceanogr.* **40**, 898–907.
50. Williams, P. J. le B. (1995) Evidence for the seasonal accumulation of carbon-rich dissolved organic material, its scale in comparison with changes in particulate material and the consequential effect on net C/N assimilation ratios. *Mar. Chem.* **51**, 17–29.
51. Leppard, G. G. (1995) The characterization of algal and microbial mucilages and their aggregates in aquatic ecosystems. *Sci. Total Environ.* **165**, 103–131.
52. Alldredge, A. L., U. Passow and B. E. Logan (1993) The abundance and significance of a class of large, transparent organic particles in the ocean. *Deep-Sea Res.* **40**, 1131–1140.
53. Passow, U. (2002) Transparent exopolymer particles (TEP) in aquatic environments. *Prog. Oceanogr.* **55**, 287–333.
54. Chin, W.-C., M. V. Orellana, I. Quesada and P. Verdugo (2004) Secretion in unicellular marine phytoplankton: Demonstration of regulated exocytosis in *Phaeocystis globosa*. *Plant Cell Physiol.* **45**(5), 535–542.
55. Engel, A. (2004) Distribution of transparent exopolymer particles (TEP) in the northeast Atlantic Ocean and their potential significance for aggregation processes. *Deep-Sea Res. I* **51**, 83–92.
56. Underwood, G. J., M. Boulcott, C. A. Raines and K. Waldron (2004) Environmental effects on exopolymer production by marine benthic diatoms: Dynamics, changes in composition, and pathways of production. *J. Phycol.* **40**, 293–304.
57. Davidson, K., E. C. Roberts and L. G. Gilpin (2002) The relationship between carbon and biovolume in marine microbial mesocosms under different nutrient regimes. *Eur. J. Phycol.* **37**, 501–507.
58. Orellana, M. V. and P. Verdugo (2003) Ultraviolet radiation blocks the organic carbon exchange between the dissolved phase and the gel phase in the ocean. *Limnol. Oceanogr.* **48**(4), 1618–1623.
59. Mari, X., F. Rassoulzadegan and C. P. D. Brussaard (2004) Role of TEP in the microbial food web structure. II. Influence on the ciliate community structure. *Mar. Ecol. Prog. Ser.* **279**, 23–32.
60. Prieto, L., F. Sommer, H. Stibor and W. Koeve (2001) Effects of planktonic copepods on transparent exopolymer particles (TEP) abundance and size spectra. *J. Plankton Res.* **23**, 515–525.
61. Passow, U. and A. L. Alldredge (1999) Do transparent exopolymer particles (TEP) inhibit grazing by the euphausiid *Euphausia pacifica*? *J. Plankton Res.* **21**, 2203–2217.
62. Alldredge, A. L., C. Gotschalk, U. Passow and U. Riebesell (1995) Mass aggregation of diatom blooms: Insights from a mesocosm study. *Deep-Sea Res. II* 32, 9–27.
63. Vernet, M. and K. Whitehead (1996) Release of ultraviolet-absorbing compounds by the red-tide dinoflagellate *Lingulodinium polyedra*. *Mar. Biol.* **127**, 35–44.
64. Sarmiento, J. L., T. M. C. Hughes, R. J. Stouffer and S. Manabe (1998) Simulated response of the ocean carbon cycle to anthropogenic climate warming. *Nature* **393**, 245–249.
65. Sarmiento, J. L., N. Gruber, M. A. Brzezinski and J. P. Dunne (2004) High-latitude controls of thermocline nutrients and low latitude biological productivity. *Nature* **427**, 56–60.